

Ultra-High Energy Cosmic Ray Nuclei from Individual Magnetized Sources

Günter Sigl†

†GReCO, Institut d'Astrophysique de Paris, C.N.R.S., 98 bis boulevard Arago,
F-75014 Paris, France

Fédération de Recherche Astroparticule et Cosmologie, Université Paris 7, 2 place
Jussieu, 75251 Paris Cedex 05, France

Abstract. We investigate the dependence of composition, spectrum and angular distributions of ultra-high energy cosmic rays above 10^{19} eV from individual sources on their magnetization. We find that, especially for sources within a few megaparsecs from the observer, observable spectra and composition are severely modified if the source is surrounded by fields of $\sim 10^{-7}$ G on scales of a few megaparsecs. Low energy particles diffuse over larger distances during their energy loss time. This leads to considerable hardening of the spectrum up to the energy where the loss distance becomes comparable to the source distance. Although details depend on the unknown magnetic field structure, magnetized sources thus have very important consequences for observations, even if observed deflections are only a few degrees. If primaries are predominantly nuclei of atomic mass A accelerated up to a maximum energy E_{\max} with spectra not much softer than E^{-2} , secondary protons from photo-disintegration can produce a conspicuous peak in the spectrum at energy $\simeq E_{\max}/A$. A related feature appears in the average mass dependence on energy.

PACS numbers: 98.70.Sa, 13.85.Tp, 98.65.Dx, 98.54.Cm

Keywords: uhc, maf

Submitted to: *Journal of Cosmology and Astroparticle Physics, JCAP*

1. Introduction

The origin of ultra-high energy cosmic rays (UHECR) above 10^{19} eV ($= 10$ EeV) is a mystery since many years [1, 2]. Several next-generation experiments, most notably the Pierre Auger experiment now under construction [3] and the EUSO project [4] are now trying to solve this mystery.

Although statistically meaningful information about the UHECR energy spectrum and arrival direction distribution has been accumulated, no conclusive picture for the nature and distribution of the sources emerges naturally from the data. There is on the one hand the approximate isotropic arrival direction distribution [5] which indicates that we are observing a large number of weak or distant sources. On the other hand, there are also indications which point more towards a small number of local and therefore bright sources, especially at the highest energies: First, the AGASA ground array claims statistically significant multi-plets of events from the same directions within a few degrees [6, 5], although this is controversial [7] and has not been seen so far by the fluorescence experiment HiRes [8]. The spectrum of this clustered component is $\propto E^{-1.8}$ and thus much harder than the total spectrum [6]. Second, nucleons above $\simeq 70$ EeV suffer heavy energy losses due to photo-pion production on the cosmic microwave background — the Greisen-Zatsepin-Kuzmin (GZK) effect [9] — which limits the distance to possible sources to less than $\simeq 100$ Mpc [10]. Heavy nuclei at these energies are photo-disintegrated in the cosmic microwave background within a few Mpc [11]. For a uniform source distribution this would predict a “GZK cutoff”, a drop in the spectrum. However, the existence of this “cutoff” is not established yet from the observations [12].

The picture is further complicated by the likely presence of large scale extra-galactic magnetic fields (EGMF) that will lead to deflection of any charged UHECR component. Magnetic fields are omnipresent in the Universe, but their true origin is still unclear [13]. Magnetic fields in galaxies are observed with typical strengths of a few micro Gauss, but there are also some indications for fields correlated with larger structures such as galaxy clusters [14]. Magnetic fields as strong as $\simeq 1\mu G$ in sheets and filaments of the large scale galaxy distribution, such as in our Local Supercluster, are compatible with existing upper limits on Faraday rotation [14, 15]. It is also possible that fossil cocoons of former radio galaxies, so called radio ghosts, contribute significantly to the isotropization of UHECR arrival directions [16].

Only recently attempts have been made to simulate UHECR propagation in a realistically structured and magnetized universe based on large scale structure simulations [17, 18]. These two simulations used different models for the EGMF: Whereas seed fields were continuously injected at shocks in Ref. [17], Ref. [18] started from uniform seed fields. In both cases, the seed field strength had to be normalized to reproduce observed rotation measures. Interestingly, the EGMF in Ref. [17] is considerably more extended and leads to much larger average deflections than in Ref. [18]. The main reason is probably due to the different EGMF models. This suggests

that the influence of EGMF on UHECR propagation is currently hard to quantify. The two works agree, however, at least in the following: First, the observer is most likely situated in a region with relatively weak EGMF, $\lesssim 10^{-9}$ G. In Ref. [17] which used an unconstrained large scale structure simulation, this was deduced from comparison of predicted and observed UHECR anisotropies, whereas in Ref. [18] this followed from their constrained simulation which is supposed to lead to an approximate model of our extra-galactic environment. Second, the fields are not strong and extended enough to allow an interpretation of the large scale isotropy of UHECR arrival directions by only one nearby source, as suggested in Ref. [19]. Finally, both these works were restricted to nucleons. Heavy nuclei may further complicate the issue and lead to large deflection even in the EGMF scenario of Ref. [18].

In the present paper we study UHECR spectra, composition and angular distribution from individual discrete sources injecting protons or nuclei into a highly structured EGMF which is significant only in the neighborhood of the source. This is different from the more idealized Monte Carlo simulations for individual sources in Refs. [20, 21, 22, 23, 24] in the following points: The EGMF in these simulations was idealized by a Kolmogorov spectrum with a possible coherent component, with a field energy density either following a Gaussian profile [22, 24] or being constant [20, 23], or as organized in spatial cells with a given coherence length and a strength depending as a power law on the local density [21]. Furthermore, the observer was immersed in fields of similar strength as the source, and these simulations were restricted to nucleons.

In the context of a highly structured EGMF it was already found that the auto-correlation function at degree scales decreases with source magnetization and can thus be used as a signature for magnetic fields [25, 17]. Here we will find that even if off-sets of arrival directions from the source direction are moderate, spectra and composition are considerably modified if the source is surrounded by EGMF of the order 10^{-7} G on scales of a few Mpc.

In Sect. 2 we describe our simulations, in Sect. 3 the results are presented, and we conclude in Sect. 4.

2. Simulations

We will specifically study two cases where the location of the observer and source are chosen from the large scale structure simulation used in Ref. [17], see Ref. [26]. In the first case the source is at a distance of 3.3 Mpc, similar to the starburst galaxy M82 or the radio galaxy Centaurus A. The field strength at the observer is $\simeq 3 \times 10^{-11}$ G, whereas the source is immersed in fields of $\sim 10^{-7}$ G. We will denote this scenario by “M82”. In the second case, the source is immersed in a galaxy cluster at 18.6 Mpc distance, reminiscent of the Virgo cluster. The field strength at the observer is $\simeq 10^{-11}$ G, whereas the source is immersed in fields of a few 10^{-7} G on scales of several Mpc. We will denote this scenario by “Virgo”. These two cases are visualized in Fig. 1. We consider the steady state situation which amounts to assuming that these sources are active on time

scales at least as long as propagation time.

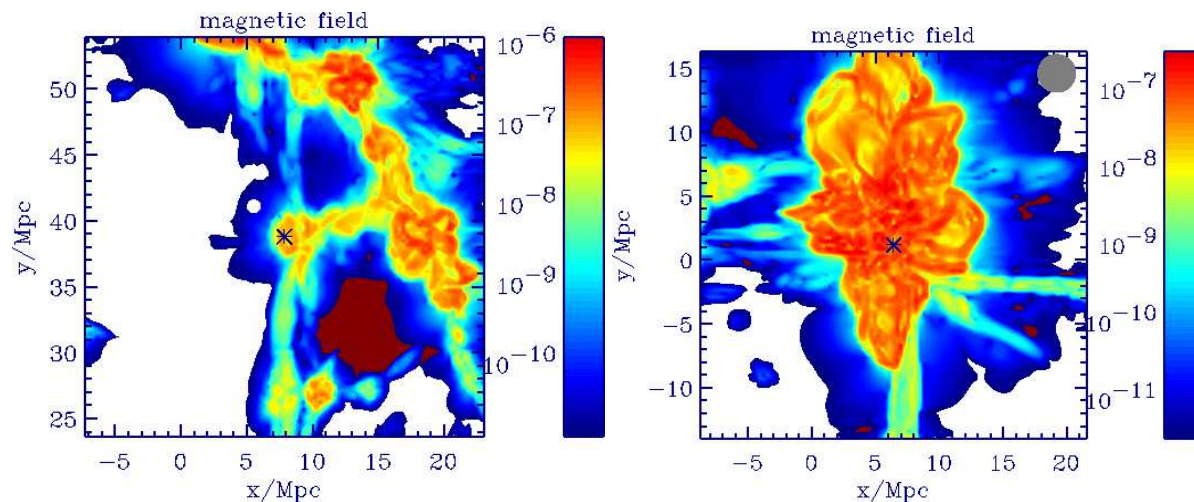


Figure 1. Log-scale two-dimensional cuts through magnetic field total strength (color scale, in Gauss) with source position indicated by the asterisk in the center. Left panel: Scenario “M82”. The observer is represented by the white disk to the left and above the source. Right panel: Scenario “Virgo”. The observer is represented by the grey disk in the upper right corner.

The trajectory simulations are performed as described in Ref. [17]. These simulations were generalized to include heavy nuclei and follow all secondary trajectories produced by photo-disintegration reactions, in the way described in Ref. [23]. Interactions taken into account thus include pair production by protons, pion production, and photo-disintegration on the combined cosmic microwave, infrared/optical and radio photon backgrounds. For the latter, standard estimates were used, see Ref. [23] for details.

For simplicity, we will assume that nuclei are accelerated with a spectrum $\propto E^{-2}$ up to a fixed maximal energy $E_{\max} = 4 \times 10^{21}$ eV, and we will restrict ourselves to either proton or iron primaries at injection. These are reasonable assumptions for radio galaxies [27]. We note that active galaxies are likely to accelerate heavy nuclei to ultra-high energies, see Refs [17, 28] for discussions.

The observer is modeled as a sphere and a trajectory is accepted and observationally relevant quantities are saved every time it crosses this sphere. For each scenario 10^6 arriving trajectories were simulated. Galactic magnetic fields lead to deflections of maximally a few tens of degrees above 10^{19} eV and can therefore be neglected as long as one is mainly interested in spectra and chemical composition.

3. Results

Fig. 2 shows the solid angle integrated spectra predicted by scenario “M82” for iron primaries, with and without EGMF and for the source position shown in Fig. 1, left panel, and a slightly different one for comparison. Fig. 3 shows the same for proton

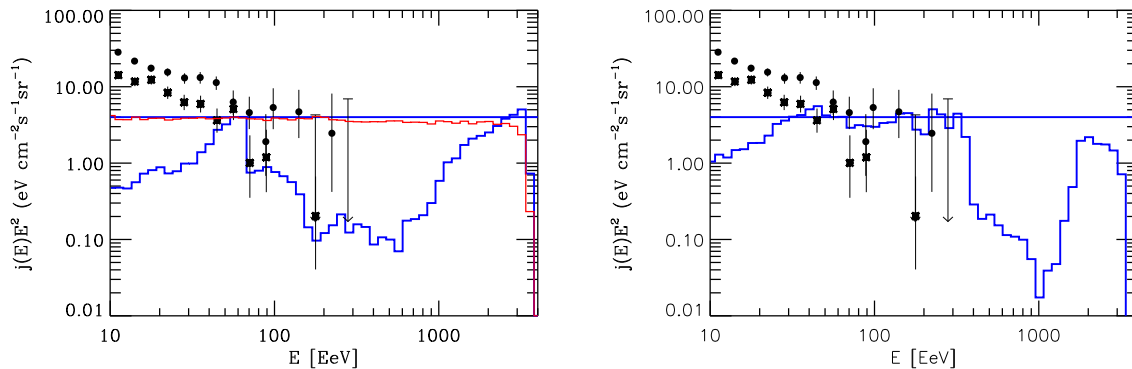


Figure 2. All-particle spectrum predicted by scenario “M82” for iron primaries with injection spectrum $\propto E^{-2.0}$ up to 4×10^{21} eV. The blue curves are for the EGMF surrounding the source as in Fig. 1, left panel, and the red curve is without EGMF. Shown for comparison are the solid angle integrated AGASA [29] (dots) and HiRes-I [30] (stars) data. The solid straight line marks the injection spectrum. The right panel is for a source off-set by about 1 Mpc from the position shown in Fig. 1, left panel. All fluxes have been normalized at 60 EeV.

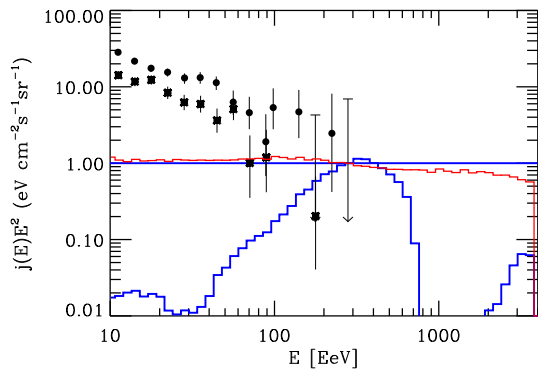


Figure 3. Same as Fig. 2, left panel, but for proton primaries. Here the fluxes have been normalized at 300 EeV.

primaries for the source position shown in Fig. 1, left panel. The normalizations are chosen such that this individual source can contribute at least partly to the measured UHECR flux at the highest energies. At lower energies cosmological sources are likely to dominate the observed flux [17].

There are several notable features for the nearby source “M82” which we will discuss in turn: It is first of all apparent that whereas without fields the spectrum is only slightly modified due to the small source distance, the magnetized case leads to a strong modification of the spectrum. This can be understood by comparing the time delay due to propagation in the EGMF, shown in Fig. 4, with typical energy loss times, shown in Fig. 5. The two time scales can indeed be comparable.

Diffusion roughly sets in once the time delay becomes comparable to the distance traveled. If the latter is not much larger than the coherence length L_c of the field of

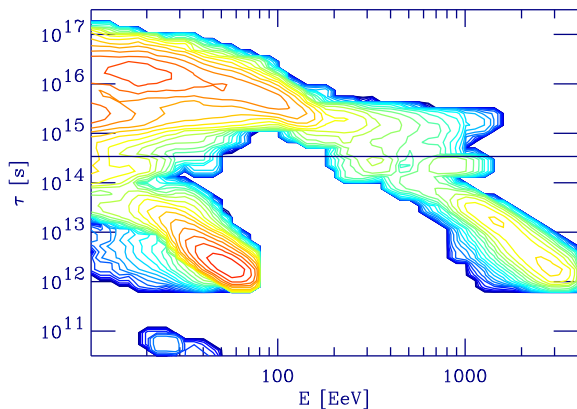


Figure 4. The distribution of time delays and arrival energies for the scenario “M82” for iron primaries, corresponding to Fig. 2, left panel. The horizontal line corresponds to the rectilinear propagation time.

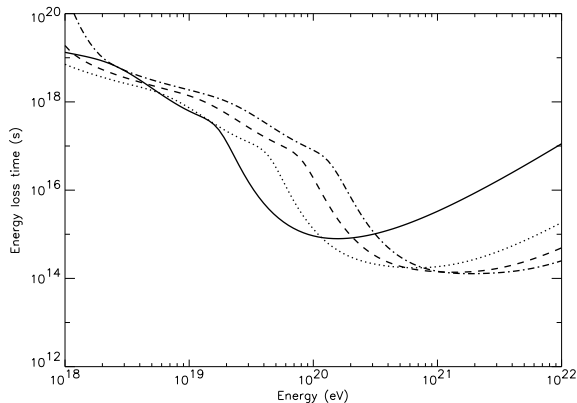


Figure 5. The energy loss time as a function of energy for photo-disintegration on the combined cosmic microwave, infra-red and radio backgrounds. The solid line is for Helium nuclei, the dotted line for Carbon, the dashed line for Silicon, and the dash-dotted line for Iron. From Ref. [23].

r.m.s. strength B , the transition from rectilinear propagation to diffusion occurs when the Larmor radius $r_L(E) \simeq E/(ZeB)$ becomes comparable to L_c , or at

$$E_c \simeq 10^{20} Z \left(\frac{B}{10^{-7} \text{ G}} \right) \left(\frac{L_c}{1 \text{ Mpc}} \right) \text{ eV}. \quad (1)$$

For $E \lesssim E_c$ the time delay scales asymptotically as $\tau(E) \propto E^{-1/3}$, whereas in the rectilinear regime $\tau(E) \propto E^{-2}$ [22]. According to Eq. (1), for light nuclei and $L_c \sim 100$ kpc this transition occurs indeed between 10^{19} eV and 10^{20} eV, consistent with what is seen in Fig. 4 for the branch with large delay times. This is consistent with the simulations of Ref. [18] which has weaker and less extended fields than used in our simulations, but where nevertheless protons diffuse in typical galaxy clusters up to several 10^{19} eV, as discussed in Ref. [31].

Another conspicuous feature in case of iron primaries is a rise of the spectrum

towards lower energies at $E \simeq 4 - 6 \times 10^{19}$ eV, see Fig. 2, whose strength depends, however, considerably on the detailed EGMF realization. This energy roughly coincides with E_{\max}/A where $A = 56$ for iron. It is thus due to the maximal energies of nucleons produced as secondaries by iron photo-disintegration. This is confirmed by the average atomic mass as a function of energy shown in Fig. 6 which shows a sharp drop at the same energy $E \simeq 6 \times 10^{19}$ eV due to these nucleons. Since these nucleons at energy E are produced by the flux of nuclei at energy AE , their effect is visible only for injection spectra not much softer than E^{-2} . The nucleon threshold also appears in a branch of events with delay times $\tau \sim 10^{12}$ s around $E \sim 60$ EeV in Fig. 4. These events are presumably related to the production of neutrons in photo-disintegration which are not deflected.

Finally, again for iron primaries, stretching over about half an order of magnitude in energy, at $E \lesssim 6 \times 10^{19}$ eV and at $E \lesssim E_{\max}$ the spectrum is considerably hardened, see Fig. 2, left panel. These two intervals are off-set from each other by roughly the charge of the iron primaries, $Z = 26$. A similar hardening is seen for proton primaries in the observed spectrum below $\simeq 3 \times 10^{20}$ eV, see Fig. 3. The hardening in these energy intervals can be interpreted by diffusive effects in terms of approximate analytical terms as follows:

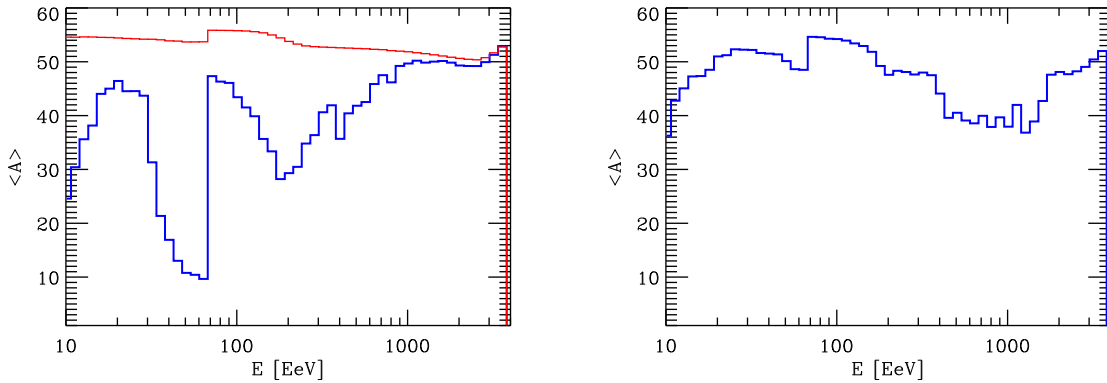


Figure 6. Average atomic mass as a function of energy predicted by scenario “M82” for iron primaries. The blue curves are for the EGMF surrounding the source as in Fig. 1, left panel, and the red curve is without EGMF. The injection parameters and source positions are as in the two panels of Fig. 2, respectively.

In the homogeneous case the diffusion - energy loss equation characterized by an energy dependent diffusion coefficient $D(E)$ and (continuous) energy losses, $dE/dt = -E/\tau_{\text{loss}}(E)$, has the solution [32, 33, 22]

$$j(E) = \frac{1}{4\pi} \int_E^{+\infty} \frac{dE'}{E} \frac{Q(E')\tau_{\text{loss}}(E)}{[4\pi\lambda(E, E')]^{3/2}} \exp\left[-\frac{d^2}{4\lambda(E, E')^2}\right], \quad (2)$$

for the flux $j(E)$. Here, $Q(E)$ is the injection spectrum of the discrete source at distance

d and

$$\lambda(E_1, E_2) \equiv \left[\int_{E_1}^{E_2} d \ln E' \tau_{\text{loss}}(E') D(E') \right]^{1/2}, \quad (3)$$

denotes an effective path length against energy losses. Since $D(E) \propto E^\alpha$ with $\alpha \lesssim 1$ [22] and $\tau_{\text{loss}}(E)$ grows quickly with decreasing energy, see Fig. 5, $\lambda(E, E')$ increases with decreasing E . This gives rise to a change of slope in the flux Eq. (2), at an energy E_t where $\lambda(E, E') \simeq d$: At energies $E \gtrsim E_t$ where $\lambda(E, E') \lesssim d$, the flux starts to become exponentially suppressed according to Eq. (2) which corresponds to the usual GZK-type cutoff. At energies $E \lesssim E_t$ the spectrum is modified by $\tau_{\text{loss}}(E)/\lambda(E, E')^3 \propto \tau_{\text{loss}}(E)^{-1/2} D(E)^{-3/2}$ relative to the injection spectrum. This represents the UHECR density proportional to the quotient of the accumulation time $\tau_{\text{loss}}(E)$ and the volume $\lambda(E, E')^3$ over which UHECR of energy E are distributed. In an EGMF with uniform statistical properties, $D(E)^{-3/2} \propto E^{-3\alpha/2}$ can increase faster with decreasing energy E than $\tau_{\text{loss}}(E)^{-1/2}$ decreases. This can lead to a *steepening* of the spectrum as observed, e.g., in the simulations of Refs. [22, 23, 34] and discussed analytically in Ref. [33]. In contrast, in our inhomogeneous scenarios the effective diffusion coefficient $\overline{D(E)}$ depends more weakly on E because lower energy particles diffuse to larger distances from the source during their larger energy loss time. The correspondingly smaller EGMF partly compensates the decrease of $\overline{D(E)}$ with E . As a consequence, the factor $\tau_{\text{loss}}(E)^{-1/2} \overline{D(E)}^{-3/2}$ in general leads to suppression with decreasing energy.

Since according to Fig. 5 the minimal $\tau_{\text{loss}}(E)$ is comparable to the source distance d in our scenarios, and $D(E) \sim r_L(E)$, the energy E_t is also roughly equal to the energy E_c , Eq. (1), where transition from diffusion to straight line propagation occurs. This provides a rough explanation of the transition from diffusive hardening to softening at higher energies seen in the spectra of Figs. 2, Fig. 3, and Fig. 8 below. It should be kept in mind, however, that our scenarios are highly inhomogeneous, the diffusion approximation strictly speaking does not apply far from the source, and these arguments can thus be considered only as approximate at best. Monte Carlo simulations are indispensable in this situation.

In order to test how much the results depend on the detailed realization of EGMF and source, we also performed simulations in which the exact source position is varied within 1-2 Mpc within the general structures shown in Fig. 1. We find that the general tendency to spectral hardening at energies where UHECR diffuse in the vicinity of the source is always seen. However, the detailed shape of the predicted observable spectra depends considerably on the concrete structure of the EGMF. This is due to magnetic lensing [35] which leads to flux enhancements along specific propagation paths at specific energies, especially if there are field lines connecting source and observer. This is consistent with the direction dependence of the simulated nucleon spectrum from a source at the center of a magnetic slab obtained in Ref. [24]. Due to the unknown magnetic field structure these spectral details are in general unpredictable. This is

demonstrated by comparing the two panels in Fig. 2 for iron primaries. The same is true for the detailed angular distributions.

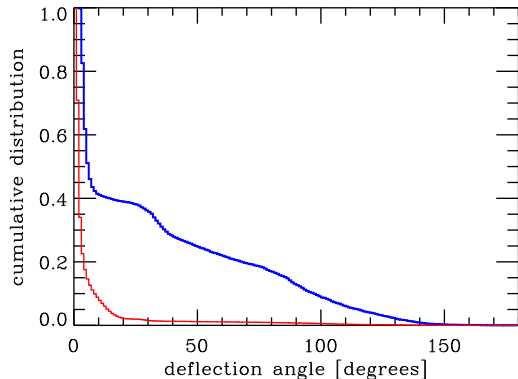


Figure 7. The cumulative distribution of arrival direction off-sets from the source direction for UHECR above 4×10^{19} eV in scenario “M82” for iron primaries, corresponding to Fig. 2, left panel (blue curve) and proton primaries, corresponding to Fig. 3 (red curve).

Fig. 6 shows the average atomic mass of observed UHECR as a function of energy for iron primaries. The nucleon spike towards low $\langle A \rangle$ at $E \simeq 6 \times 10^{19}$ eV is clearly visible, as discussed above. Below that energy there appears, however, also a relatively heavy component which survived excessive photo-disintegration. At all energies, the EGMF reduces the average atomic number due to increased photo-disintegration compared to undeflected propagation. Apart from this and the energy of the nucleon spike, the detailed mass distribution is, however, quite sensitive to the EGMF structure, as seen by comparing the two panels in Fig. 6.

Fig. 7 shows the cumulative distribution of arrival direction off-sets from the source direction for the same “M82” scenario. Clearly, deflections are larger for iron primaries, whereas for proton primaries they are only a few degrees.

Table 1. Approximate source emission power above $\sim 10^{19}$ eV in erg/s corresponding to the normalizations of the observed spectra in Figs. 2, left panel, 3, and 8.

	with EGMF	no EGMF
M82, iron primaries	2.8×10^{40}	6.6×10^{40}
M82, proton primaries	3.8×10^{39}	1.7×10^{40}
Virgo, iron primaries	3.9×10^{42}	2.4×10^{42}
Virgo, proton primaries	2.0×10^{42}	1.7×10^{42}

We can also extract from the simulations the necessary source power corresponding to a particular normalization of the observed spectrum. For the normalizations shown in Figs. 2, 3, and 8 below the source power is given in Tab. 1. The required power is not strongly changed by the presence of the EGMF because we have normalized at the

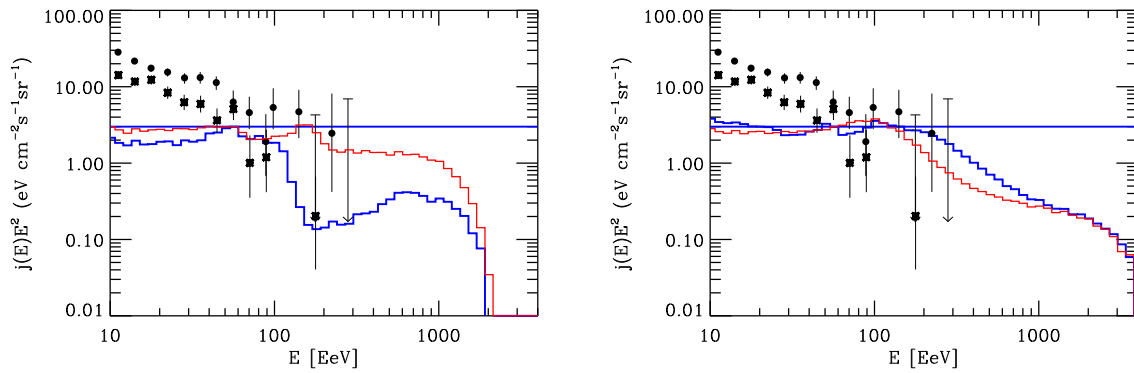


Figure 8. Same as Figs. 2 and 3 but for scenario “Virgo”. The left and right panels are for iron and proton primaries, respectively. All fluxes have been normalized at 60 EeV.

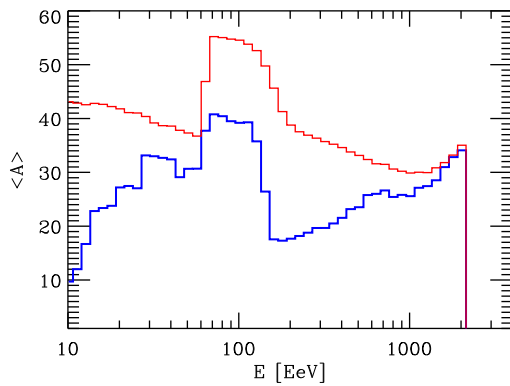


Figure 9. Same as Fig. 6, but for scenario “Virgo”.

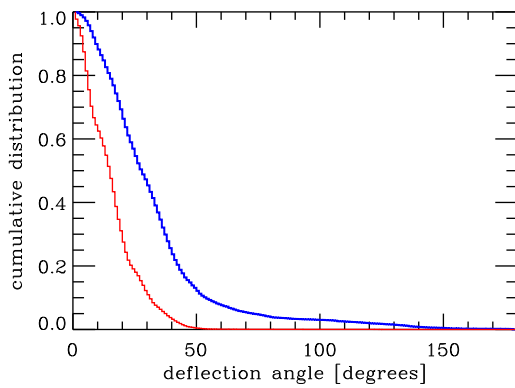


Figure 10. Same as Fig. 7, but for scenario “Virgo”. This corresponds to the cases shown in Fig. 8.

energy where the energy flux, which is proportional to the y-axis in Figs. 2, 3 and 8, is maximal. Note that for a given normalization of the observed spectrum, iron primaries

require a somewhat higher injection power because a higher fraction of the injected energy is degraded below 10^{19} eV during propagation due to spallation. For the case of “M82” most of the difference in required injection power between proton and iron primaries is due to the difference in normalization of the observed spectrum in these two cases, compare Figs. 2 and 3. Finally, the unknown EGMF structure translates into uncertainties in the required power of about an order of magnitude. Given these uncertainties of the injection spectrum and its continuation below 10^{19} eV, these values are consistent with the UHECR emission power of active galaxies discussed in this context [27], such as for M87, the main radio galaxy in the Virgo cluster [36].

Figs. 8, 9, and 10 show spectra, atomic mass distribution, and the cumulative deflection angle distribution, respectively, for the “Virgo” scenario. For direct comparison with the “M82” scenario, the same injection parameters have been assumed. The effects of the EGMF surrounding the source, although more extended than in the scenario “M82”, are here relatively smaller. This is because the delay time relative to the straight line propagation time now only reaches a maximum of ~ 10 at $\simeq 10^{19}$ eV, compared to ~ 100 in the scenario “M82”. The EGMF effects are, however, still significant and show the same generic features as discussed for the case “M82”. In fact, for the same injection spectrum, at low energies, the suppression of the average atomic mass due to increased photo-disintegration by propagation in the EGMF is more severe than for the more nearby source “M82”, compare Figs. 6 and 9. This is because due to the larger propagation distance, fewer nuclei survive spallation.

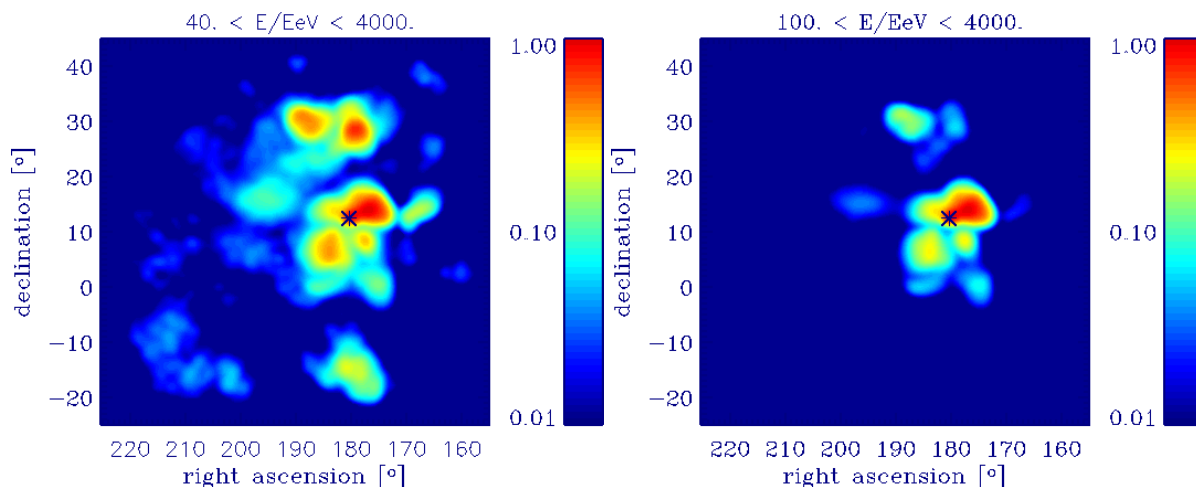


Figure 11. Sky distribution of UHECR arrival directions above 4×10^{19} eV (left panel) and above 10^{20} eV (right panel) for proton primaries in scenario “Virgo”. The source position is marked by an asterisk. The angular resolution was assumed to be 1° .

Note that the conventional pile-up in the spectrum around 100 EeV is clearly visible in the case of proton primaries without EGMF, see Figs. 3 and 8, right panels.

Fig. 11 shows an actual sky plot of arrival directions of events above 4×10^{19} eV and above 10^{20} eV for proton primaries in scenario “Virgo”. Several distinct images are

clearly seen which suggests significant magnetic lensing [35] in the EGMF structure from Fig. 1, right panel. This is not surprising given the fact that lensing in general sets in at energies higher than the transition energy to diffusion which, according to Eq. (1), is roughly around 10^{20} eV. The number of images and the deflection angles decrease with increasing energy, but are still significant at 10^{20} eV and can be resolved with sufficient statistics.

4. Conclusions

We investigated the impact of Mpc-scale magnetic fields of $\sim 10^{-7}$ G strength surrounding ultra-high energy cosmic ray sources on cosmic ray observations above 10^{19} eV for the likely case that magnetic fields within a few Mpc around Earth are insignificant. We find that such source fields can strongly modify spectra and composition at Earth, especially for nearby sources for which the fields can considerably modify propagation times relative to both energy loss and photo-disintegration time scales and to the undeflected propagation time. We found the following generic features:

The spectra are considerably hardened relative to the injection spectrum at energies below the usual GZK-like cutoff where energy loss distance and source distance become comparable. This is caused by an interplay between diffusion and energy loss: The flux of low energy particles is suppressed because diffusion spreads them out over a larger volume due to their much larger energy loss times. This is in contrast to the case of uniformly distributed magnetic fields which in general lead to a steepening of the cosmic ray flux below the GZK-cutoff. A hardened sub-GZK spectrum from individual sources would be consistent with hints of a hard clustered component in the AGASA data between 10^{19} eV and 10^{20} eV [6].

Furthermore, for a nucleus of atomic mass A as injected primary, due to the kinematics of the photo-disintegration reactions a nucleon peak appears at energy $\sim E_{\text{max}}/A$, where E_{max} is the maximal injection energy. This effect is the more prominent the harder the injection spectrum. We also found that the details of spectra and composition depend significantly on the unknown details of the magnetic fields and the position of the source therein and can thus not be predicted.

Our simulations finally show that even for iron primaries, extra-galactic magnetic fields from large scale structure simulations are not strong and extended enough to explain the observed large scale isotropy of ultra high energy cosmic ray arrival direction in terms of a single nearby source. This would require more homogeneous fields such as in Ref. [28].

Next generation experiments such as the Pierre Auger Observatories [3] and the EUSO project [4] will accumulate sufficient statistics to establish spectra and distributions of composition and arrival directions from individual sources. A potentially strong influence of magnetic fields surrounding individual sources should thus be kept in mind when interpreting data from these experiments. This is true even if source magnetic fields do not lead to strong off-sets of ultra-high energy cosmic ray arrival

directions from the source position.

Acknowledgments

This work partly builds on earlier collaborations with Gianfranco Bertone, Torsten Enßlin, Claudia Isola, Martin Lemoine, and Francesco Miniati. I am grateful to Francesco Miniati for comments on the manuscript. Luis Anchordoqui and Haim Goldberg are acknowledged for discussions on propagation of nuclei in magnetic fields. I thank the Max-Planck Institut für Astrophysik where part of this work was done for hospitality.

References

- [1] for recent reviews see P. Bhattacharjee and G. Sigl, Phys. Rept. **327**, 109 (2000) [arXiv:astro-ph/9811011]. J. W. Cronin, Rev. Mod. Phys. **71**, S165 (1999); M. Nagano and A. A. Watson, Rev. Mod. Phys. **72**, 689 (2000); A. V. Olinto, Phys. Rept. **333**, 329 (2000) [arXiv:astro-ph/0002006]; X. Bertou, M. Boratav and A. Letessier-Selvon, Int. J. Mod. Phys. A **15**, 2181 (2000) [arXiv:astro-ph/0001516]; G. Sigl, Science **291**, 73 (2001); F. W. Stecker, J. Phys. G **29**, R47 (2003) [arXiv:astro-ph/0309027].
- [2] “Physics and Astrophysics of Ultra High Energy Cosmic Rays”, Lecture Notes in Physics, **576** (Springer Verlag, 2001), eds. M. Lemoine, G. Sigl.
- [3] J. W. Cronin, Nucl. Phys. Proc. Suppl. **28B**, 213 (1992); The Pierre Auger Observatory Design Report (ed. 2), March 1997; see also <http://www.auger.org>.
- [4] See <http://www.euso-mission.org>.
- [5] W. S. Burgett and M. R. O’Malley, Phys. Rev. D **67**, 092002 (2003) [arXiv:hep-ph/0301001].
- [6] M. Teshima et al., Proc. 28th International Cosmic Ray Conference, Tsukuba, Japan, **1**, 437 (2003).
- [7] C. B. Finley and S. Westerhoff, arXiv:astro-ph/0309159.
- [8] C. B. Finley et al., Proc. 28th International Cosmic Ray Conference, Tsukuba, Japan, **1**, 433 (2003).
- [9] K. Greisen, Phys. Rev. Lett. **16**, 748 (1966); G. T. Zatsepin and V. A. Kuzmin, JETP Lett. **4**, 78 (1966) [Pisma Zh. Eksp. Teor. Fiz. **4**, 114 (1966)].
- [10] F. W. Stecker, Phys. Rev. Lett. **21**, 1016 (1968).
- [11] J. L. Puget, F. W. Stecker and J. H. Bredekamp, Astrophys. J. **205**, 638 (1976); L. N. Epele and E. Roulet, Phys. Rev. Lett. **81**, 3295 (1998) [arXiv:astro-ph/9806251]; L. N. Epele and E. Roulet, JHEP **9810**, 009 (1998) [arXiv:astro-ph/9808104]; F. W. Stecker, Phys. Rev. Lett. **81**, 3296 (1998); F. W. Stecker and M. H. Salamon, Astrophys. J. **512**, 521 (1992) [arXiv:astro-ph/9808110].
- [12] D. R. Bergman, Proc. 28th International Cosmic Ray Conference, Tsukuba, Japan, **1**, 397 (2003).
- [13] for reviews see, e.g., P. P. Kronberg, Rept. Prog. Phys. **57**, 325 (1994); D. Grasso and H. R. Rubinstein, Phys. Rept. **348**, 163 (2001) [arXiv:astro-ph/0009061].
- [14] J. P. Vallée, Fundamentals of Cosmic Physics **19**, 1 (1997); J. L. Han and R. Wielebinski, arXiv:astro-ph/0209090.
- [15] D. Ryu, H. Kang, and P. L. Biermann, Astron. Astrophys. **335**, 19 (1998).
- [16] G. A. Medina-Tanco and T. A. Ensslin, Astropart. Phys. **16**, 47 (2001) [arXiv:astro-ph/0011454].
- [17] G. Sigl, F. Miniati and T. A. Ensslin, arXiv:astro-ph/0401084.
- [18] K. Dolag, D. Grasso, V. Springel and I. Tkachev, arXiv:astro-ph/0310902.
- [19] G. R. Farrar and T. Piran, arXiv:astro-ph/0010370.

- [20] G. Sigl, M. Lemoine and A. V. Olinto, Phys. Rev. D **56**, 4470 (1997) [arXiv:astro-ph/9704204]; G. Sigl and M. Lemoine, Astropart. Phys. **9**, 65 (1998) [arXiv:astro-ph/9711060].
- [21] G. A. Medina-Tanco, Astrophys. J. **495**, L71 (1998) [arXiv:astro-ph/9801060].
- [22] G. Sigl, M. Lemoine and P. Biermann, Astropart. Phys. **10**, 141 (1999) [arXiv:astro-ph/9806283].
- [23] G. Bertone, C. Isola, M. Lemoine and G. Sigl, Phys. Rev. D **66**, 103003 (2002) [arXiv:astro-ph/0209192].
- [24] T. Stanev, arXiv:astro-ph/0303123; T. Stanev, D. Seckel and R. Engel, Phys. Rev. D **68**, 103004 (2003) [arXiv:astro-ph/0108338]; T. Stanev, R. Engel, A. Mucke, R. J. Protheroe and J. P. Rachen, Phys. Rev. D **62**, 093005 (2000) [arXiv:astro-ph/0003484].
- [25] G. Sigl, F. Miniati and T. A. Ensslin, arXiv:astro-ph/0309695.
- [26] F. Miniati, Mon. Not. Roy. Astron. Soc. **337**, 199 (2002) [arXiv:astro-ph/0203014].
- [27] J. P. Rachen and P. L. Biermann, Astron. Astrophys. **272**, 161 (1993) [arXiv:astro-ph/9301010]; J. P. Rachen, T. Stanev and P. L. Biermann, Astron. Astrophys. **273**, 377 (1993) [arXiv:astro-ph/9302005].
- [28] L. Anchordoqui, H. Goldberg, S. Reucroft and J. Swain, Phys. Rev. D **64**, 123004 (2001) [arXiv:hep-ph/0107287].
- [29] M. Takeda *et al.*, Phys. Rev. Lett. **81**, 1163 (1998) [arXiv:astro-ph/9807193]; M. Takeda *et al.*, Astrophys. J. **522**, 225 (1999) [arXiv:astro-ph/9902239]; N. Hayashida *et al.*, arXiv:astro-ph/0008102; see also <http://www-akeno.icrr.u-tokyo.ac.jp/AGASA/>.
- [30] T. Abu-Zayyad *et al.* [High Resolution Fly's Eye Collaboration], arXiv:astro-ph/0208243; T. Abu-Zayyad *et al.* [High Resolution Fly's Eye Collaboration], arXiv:astro-ph/0208301.
- [31] C. Rordorf, D. Grasso and K. Dolag, arXiv:astro-ph/0405046.
- [32] S. I. Syrovatskii, Sov. Astron. **3**, 22 (1959); see also V. S. Berezinsky, S. V. Bulanov, V. A. Dogiel, V. L. Ginzburg, and V. S. Ptuskin, *Astrophysics of Cosmic Rays* (North-Holland, Amsterdam, 1990).
- [33] R. Aloisio and V. Berezinsky, arXiv:astro-ph/0403095.
- [34] M. Lemoine, G. Sigl and P. Biermann, arXiv:astro-ph/9903124.
- [35] D. Harari, S. Mollerach, E. Roulet and F. Sanchez, JHEP **0203**, 045 (2002) [arXiv:astro-ph/0202362].
- [36] R. J. Protheroe, A. C. Donea and A. Reimer, Astropart. Phys. **19**, 559 (2003) [arXiv:astro-ph/0210249].